QUANTIFYING CHANGES IN WEAK LAYER MICROSTRUCTURE ASSOCIATED WITH LOADING EVENTS

Eric Lutz [1]*, Karl Birkeland[1,2], Hans-Peter Marshall[3,4], Kathy Hansen[1]
[1]Montana State University, Bozeman, Montana
[2]USDA Forest Service National Avalanche Center,, Bozeman, Montana
[3]Center for Geophysical Investigation of the Shallow Subsurface, Boise State University, Boise, ID.
[4]Cold Regions Research and Engineering Laboratory

ABSTRACT: Researchers and practitioners have long utilized a variety of penetrometers to investigate the snowpack. Identifying definitive relationships between penetrometer-derived microstructural information and stability has been challenging. The purpose of this study is two-fold: 1. We propose a simple field test that can be implemented by the scientific community to establish relationships between load and penetrometer-derived microstructural strength, 2. Utilizing the SnowMicroPen (SMP) data, we quantify changes in weak layer residual strength and structural dimensions associated with a loading event. Our dataset is from Moonlight Basin, Montana and includes three modified loaded-column tests, each paired with 5 SMP profiles. Depth hoar comprised the targeted weak layer. Results indicate that loading events cause the residual bond strength and bond frequency in large-grained weak layers to decrease significantly. Much like a compression test at a micro-scale, the force required for the SMP to rupture individual bonds as well as the micro-strength decrease significantly when the slab stress is increased by artificially adding blocks of snow. A decrease in observed bond frequency within the weak layer (or an increase in the distance between bonds) also occurs after a loading event, probably because some bonds within the weak layer have already failed or are so close to failing that the penetrometer cannot detect their rupture. Artificial removal of slab stress resulted in greater rupture forces and distances between bonds, likely due to elastic rebound. This indicates that long after a natural loading event has occurred, elastic deformation still exists within the weak layer.

KEYWORDS: Microstructure, Stability, Loading event, SnowMicroPen.

1. INTRODUCTION

Avalanche forecasting involves the integration of stability, snowpack and meteorological factors (McClung and Schaerer, 1993). Of these three classes, direct stability observations such as recent avalanche activity and collapsing, and slope stability tests provide invaluable information about current instabilities. Snow hardness on the other hand, which has long been recognized as an important proxy in determining the structure and strength of mountain snowpacks (e.g. Welzenbach, 1930; Paulcke, 1938; in Pielmeier, 2003:12-17), has been considered a less conclusive predictor of stability.

Researchers developed a variety of penetrometers - ranging from manual to mechanical to digital - with the long-term goal of

_____

* *Corresponding author address:* Eric Lutz, 724 South Tracy Avenue, Bozeman, MT, USA 59715; tel: 406-599-2107; email: snowscience@gmail.com

efficiently and objectively deriving stability information from resistance profiles (e.g. Bader et al., 1939; DeQuervain, 1950; Bradley, 1966: Dowd & Brown, 1986; Brown & Birkeland, 1990). In the late 1990's, building conceptually on Dowd and Brown's Digital Resistograph, Schneebeli and Johnson developed the SnowMicroPen (SMP) to record penetration resistance at force and stratigraphic resolutions that enable grain and bond-scale strength properties to be examined (Schneebeli and Johnson, 1998; Schneebeli et al., 1999).

Previously published SMP field studies have measured natural instabilities of undisturbed snow. Opportunities to test instabilities directly following loading events are limited in a given season and region by: (1) the presence of weak layers, (2) the number of critical loading events, (3) the logistical challenges of timing field campaigns to precede and coincide with a loading event and, (4) the real possibility of collapsing the weak layer while sampling. In part because of these factors, direct correlations between penetration hardness, micro-structural estimates, and

snowpack strength and stability have proven challenging (Birkeland et al., 2003; Kronholm, 2004; Lutz et al., 2007; Pielmeier et al., 2006). Developing relationships between loading events and resultant changes in microstructure will require more types of instabilities to be examined.

In this study we increase the instability of the snowpack by artificially loading an existing weakness using a modified loaded column test. The forced instability can then be recorded with the SMP to derive microstructural estimates of the weak layer's residual strength under the applied overburden. Multiple loads can be applied to a given weak layer, allowing for many scenarios to be tested. This allows us to broaden our datasets relating microstructure to slope instabilities even in the momentary absence of backcountry instabilities.

2. METHODS

2.1 *Field Method*

We collected field data on 28 March 2008 at Moonlight Basin's *Corner Pocket* where depth hoar subsisted under an ice crust and wind slab. The depth hoar layer was approximately 10 cm thick, with a series of thick crusts and compressed depth hoar below. It consisted of well-preserved depth hoar crystals ranged from 6 to 10 mm in size and formed 10 to 30 mm columns (5dh, Colbeck et al., 1990).

A temperature gradient of 8° C m^{-1} existed within the upper 5 cm of depth hoar (directly under the slab). Moonlight Basin Ski Patrol recorded 39 mm water equivalent accumulating over the 10 preceding days (Spence, pers. comm.).

Observations included three modified loaded column tests, each paired with five SMP profiles (grey dots in Figure 1, left). Column II's unaltered slab represented the natural load. Based on a practice test, we loaded Column III nearly to failure using blocks from the top of Column I and additional blocks. After isolating the backside of the columns, we made SMP measurements into the lower portion of the columns.

Since the columns were situated on an inclined slope and the SMP is generally driven perpendicular through stratigraphy, the operator drove the probe obliquely through the face of the columns, carefully positioning the SMP close to the columns without unintentionally scraping the bipod legs on the column corners. We recorded SMP measurements in sets of three, one in each column (first set of three SMP measurements are denoted with numbers and arrows in Figure 1). This sequence allowed the examination of changes occurring in any column during the sampling duration of approximately 35 minutes.

After completing SMP measurements we dynamically loaded each column until failure, using standard compression test (CT) force loads (Greene et al., 2004). While the observed
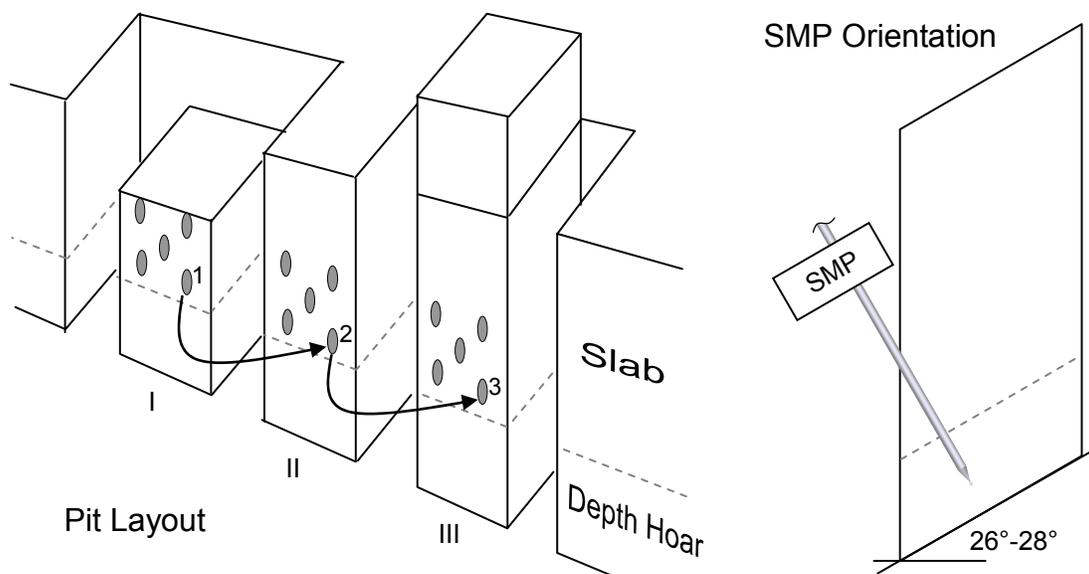
Figure 1: Pit sample layout. We isolated three 30 cm x 30 cm columns with different loads (I, II, and III) and recorded weak layer strength with the SMP. One set of SMP profiles included a profile from each column (arrows). Actually spacing between columns was greater than depicted (ca. 30 cm).

CT values provide additional stability information, the SMP probe holes likely affected the test results for all columns. After failure, we sectioned and placed each column into a large nylon duffle bag and weighed them using a fish scale, eliminating the need for time-consuming density measurements to calculate slab stress.

2.2 Delineation of Slab - Depth Hoar Transition

To allow estimates from different SMP profiles to be compared visually and statistically, we manually delineated the transition from slab to depth hoar. Such manual delineations are typical for SMP research (e.g. Kronholm, 2004). Every SMP profile exhibited the interface of interest, observed as an abrupt decrease in mean resistance and increase in local variance. Profile depths were then normalized to this reference depth.

2.3 Microstructural estimates

We estimated three microstructural properties of the weak layer using Marshall and Johnson's (submitted) micromechanical model: the mean rupture force normal to sensor tip f, the structural element length L and the micro-strength S. These estimates are derived from rupture size and frequency information recorded within SMP profiles. Excluding drops in resistance smaller than 0.032 N eliminated possible instrumental noise. Lutz (in preparation) derived this threshold value from air pocket segments of 55 SMP profiles, where he eliminated 99 % of all drops in these segments with this threshold value.

The mean rupture force f (N) is the sum of all rupture values divided by their frequency. The structural element length L (mm) is the cubic root of the average volume occupied by structures and is inversely related to bond or structure frequency. Lastly, by dividing f by L^2 we estimate the micro-strength S (N/mm^2) which describes the relationship between strength and structure.

Marshall and Johnson's (submitted) micromechanical model modifies Johnson's and Schneebeli (1999) model by accounting for limitations of the one-dimensional force signal and its force and depth resolution. The modifications include: (1) accounting for simultaneous ruptures, (2) building on Sturm et al.'s (2004) approach, the deflection at rupture δ is calculated exactly, (3) δ is calculated using individual rupture forces, (4) a force digitization

error at rupture is corrected. Cumulatively, these modifications improve the accuracy of microstructural estimates in simulations (Marshall and Johnson, submitted).

2.4 Moving-window application of estimates

For graphic visualizations of microstructural profiles, a moving-window routine calculated microstructural estimates within 5 mm windows that overlapped adjacent windows by 90 percent. For boxplots and statistical testing of the weak layer, we sampled the weak layer portion of the moving-window estimates such that no two samples were derived from the same segment of SMP profiles. Hence, each profile provided 20 independent samples, resulting in 100 samples per test column.

2.3 Analysis

Graphical and statistical comparisons allowed us to investigate associations between slab stress and weak layer properties. Boxplots visualize changes in microstructural properties. Black squares represent median values, boxes depict the inter-quartile range, legs extend to minima and maxima, and triangles depict non-parametric confidence intervals. White triangles indicate significant differences in centrality between adjacent boxes, as tested with the Wilcoxon Test. Bracketed values represent the number of sampled 5 mm segments.

The non-parametric Wilcoxon Test quantitatively tested for differences in centrality of microstructural properties between columns and between profiles. Column comparisons identify general differences associated with load changes, which can be rationalized in the context of changing snowpack stability. Each column possessed 100 samples. Profile comparisons help determine: (1) if a time-effect is evident over the sampling period, (2) the effectiveness of using individual SMP profiles to distinguish changes specifically relating to the artificial loading event.

3. RESULTS AND DISCUSSION

3.1 Compression Tests

Compression test scores reflected the load differences (Table 1). The weak layer under the artificially reduced slab (Column I) scored slightly higher CT values than did

Column II. Column III fractured with at a much lower loading step than the other columns and it also produced a Quality 1 shear (Table 1).

Table 1. Compression test field observations.

Property	Column		
	I	II	III
Description	Reduced load	Natural load	Increased load
Slab Mass (kg)	8.1	15.6	25.8
Slope Angle (°)	26.5	27.5	28
CT Score	23	20	5
Fracture Quality	2	2	1

3.2 *Slab stress (Pa) and scaled force (N)*

Artificial changes in slab thickness caused slab stress to vary dramatically between the three columns (Part 1 of Table 2). Since the columns were within 30 cm of each other and original slab thickness did not vary between columns, the difference in applied stress is largely the result of the artificial changes rather than spatial variability. Compared with Column II, Column I had an artificial vertical load reduction of approximately 900 Pa and Column III experienced an artificial vertical load increase of approximately 1300 Pa.

To compare the slab stresses with SMP-derived rupture force estimates (Section 3.3), we converted the slab stresses (Pa) to scaled force values (N) by multiplying the slab stresses by the SMP sensor tip's cross-sectional area

$(1.96 \times 10^{-5} \text{ m}^2)$ and calculated the differences between the columns (Part 2 of Table 2). The decreased load on Column I reduced the natural slab's vertical force component by 0.018 N (Part 2 of Table 2). The artificial load on Column III resulted in a 0.026 N increase in the vertical force at the SMP sensor tip-scale.

3.3 *Mean Rupture Force f (N)*

The weak layer's mean rupture force was smallest under the artificial load and greatest under the reduced load (Part 3 of Table 2; Figures 2 and 3). On average the SMP ruptured bonds with 0.0486 N less force when we increased the overburden on the weak layer This change in residual strength is of the same magnitude as the increase in scaled slab force (0.026 N, Part 2 of Table 2).

When we consider the differences in distributions evident in Figure 3, an *f* value of 0.145 N differentiates 75 % of Column III's samples from 90 % and 77 % of the samples from Columns I and II, respectively. This indicates that *f* differentiates most of the unstable samples from the stable samples and may be useful for characterizing other instabilities.

Column I possessed significantly higher rupture forces than Column II, with an average difference of 0.022 N. While the decrease in mean rupture force in Column III can be explained as a decrease in residual bond strength, the increase in strength of the

Table 2. Slab stress (Part 1), sensor-tip scaled slab force (Part 2), and SMP-derived microstructural estimates of the weak layer (Part 3), for test columns I through III. Italicized numbers in parenthesis are p-values from the Wilcoxon Test, indicating whether a significant difference in central tendency existed between two columns.

Property	Columns			Change: Natural → Unloaded		Change: Natural → Loaded	
	I (unloaded)	II (natural)	III (loaded)	Col.I – Col.II		Col.III – Col.II	
Part 1. Slab Stresses				Δ		Δ	
Shear (Pa)	393	773	1320	-380		547	
Normal (Pa)	788	1484	2483	-696		999	
Vertical (Pa)	984	1886	3185	-902		1299	
Part 2. SMP Tip-Scaled Slab Forces				Δ		Δ	
Shear (N)	0.0077	0.0152	0.0259	-0.008		0.011	
Normal (N)	0.0155	0.0291	0.0488	-0.014		0.020	
Vertical (N)	0.0193	0.0370	0.0625	-0.018		0.026	
Part 3. Microstructural Estimates				Δ	*p-value*	Δ	*p-value*
f_{median}	0.1936	0.1717	0.1232	0.0219	*(2.21E-02)*	-0.0486	*(0.00E+00)*
L_{median}	1.0394	0.9857	1.1853	0.0468	*(3.49E-04)*	0.1938	*(5.64E-20)*
S_{median}	0.1263	0.1228	0.0601	0.0004	*(9.70E-01)*	-0.0885	*(0.00E+00)*

unloaded column may be caused by rebound from elastic deformation. If a component of elastic deformation existed under the natural load, removing a large portion of the natural slab may allow the structures to rebound elastically to a less stressed (and strained) state. To know definitively if new snow caused most of the elastic deformation, we would have to test the effects of removing only the new snow from Column I.

Mean Rupture Force *f (N)*
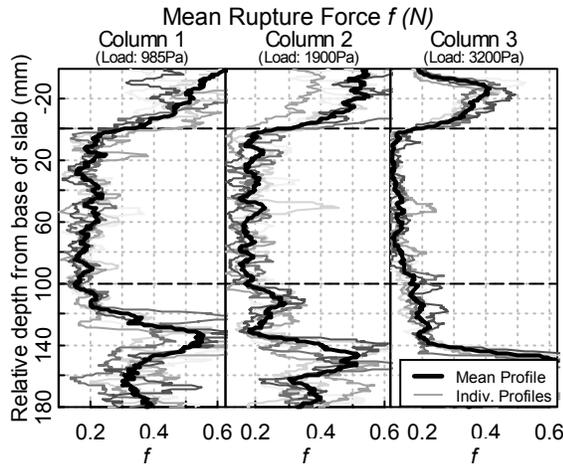
Figure 2. Profiles of the mean rupture force *f* indicate that the smallest *f* occurs within the within the depth hoar and coincides with the greatest overburden. Horizontal lines approximate depth hoar boundaries.
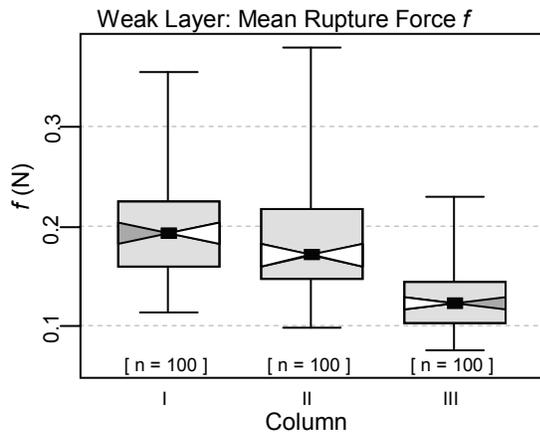
Figure 3. Mean rupture force *f* of weak layer. The unloaded column (I) possessed the highest average *f* values while the loaded column (III) maintained the smallest values

Under this new circumstance, slightly more force would be required for the SMP to rupture these structures because they are less elastically strained, resulting in slightly higher rupture forces. The increase in rupture force is

very close to the change in slab stress scaled to the sensor tip (0.018 N, Table 2). In nature this could relate to increases in stability directly following wind scour events.

3.4 Structural Element Length L (mm)

Adding an artificial load increased the structural element length *L* 0.2 mm within the weak layer (Part 3 of Table 1; Figures 4 and 5). We hypothesize that under the increased load some bonds within the weak layer have begun to fail or are so close to failing that we cannot differentiate their rupture from instrumental noise. With fewer ruptures being recognized by the penetrometer within a set volume, *L* increases.

Microstructural Element Length *L (mm)*
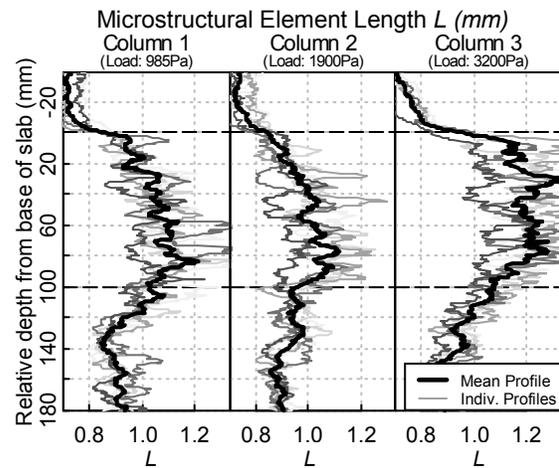
Figure 4. Microstructural element length *L*. Horizontal lines approximate depth hoar boundaries.

Interestingly, a slight increase in *L* also occurs when the slab stress is artificially reduced, as evident from Column I (Part 3 of Table 2; Figures 4 and 5). Since stress has been removed from this column, and *f* has increased, it is possible that this increase in *L* is a direct result of elastic rebound. Under the decreased slab stress, elastic deformation is released and slightly bent columnar depth hoar structures 'stand taller' than when stressed by natural or artificial loads.

When we consider the differences in distributions evident in Figure 5, an *L* value of 1.09 mm differentiates 75 % of Column III's samples from 82 % and 68 % of the samples from Columns I and II, respectively. While *L* differentiates most of the unstable samples from the stable samples it is less effective than *f.*

Unlike *f*, *L* increases when slab loads increase or decrease, albeit caused by different phenomena. Thus, *L* cannot stand alone as an indicator of a change in strength or stability.
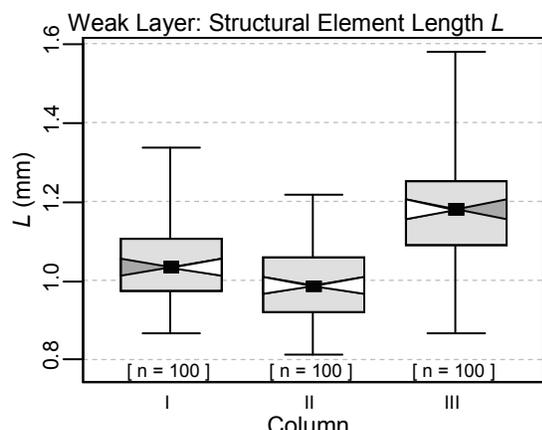
Figure 5. Microstructural element length *L*. The loaded column (III) possessed the highest *L* values and the natural column (II) maintained the smallest *L* values

3.5 *Micro-scale Strength S (N/mm^2)*

The micro-scale strength (f/L^2), yields interesting differences between the loaded and unloaded columns. While S drops significantly under the increased load on Column III, it remains unchanged by the decreased load on Column I (Figures 6 and 7). This shows us that if *f* decreases and *L* increases, as observed for the loaded column, *S* becomes small, which we would expect. If, on the other hand, *f* and *L* both increase, *S* does not change dramatically because the higher residual strength is distributed over slightly larger structure lengths (or fewer bonds per volume).

Micro-strength *S* may prove very useful in characterizing changes in weak layer strength (Figure 7). An *S* value of 0.112 N/mm^2 differentiates 75 % of Column III's sample values from 91 % and 93 % of the sampled micro-strength values from Columns I and II. This indicates that *S* alone very effectively distinguishes the loaded weak layer from the natural and unloaded weak layers. Pielmeier and Marshall (2008, this issue) found this parameter to be the most significant in distinguishing Rutschblock stablility. This parameter distinguishes Column III data (unstable, CT=5) from Column I and II data (stable, CT=23, 20) with much more accuracy than f and L alone.
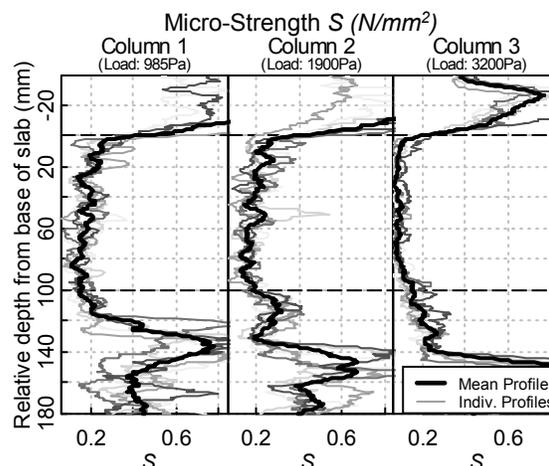
Figure 6. Micro-scale strength *S*. Horizontal lines approximate depth hoar boundaries.
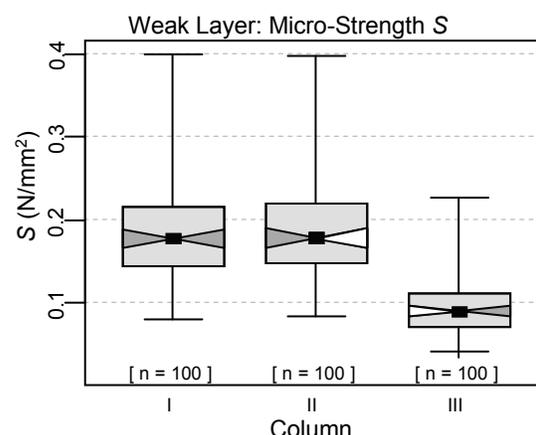
Figure 7. Micro-scale strength *S* (N/mm^2) of weak layer. The loaded column (III) possessed the lowest *S* values while the unloaded and natural columns (I and II) were indistinguishable.

3.6 *Time-Effect on Weak Layer Properties*

No changes were evident in micro-strength of Columns I and II. In Column III however, *S* increased significantly over the 35 minute sampling duration (Figure 8), mainly due to a decrease of *L*. This indicates that distances between structures have become smaller, or that bonds near failure regained strength. In either case, at the micro-scale, some amount of strengthening appears to have occurred in Column III. Caution is needed in this interpretation since each time is represented by 20 samples from a single SMP profile which may have been influenced by the pre-existing holes.

Weak Layer: Micro-Strength *S*
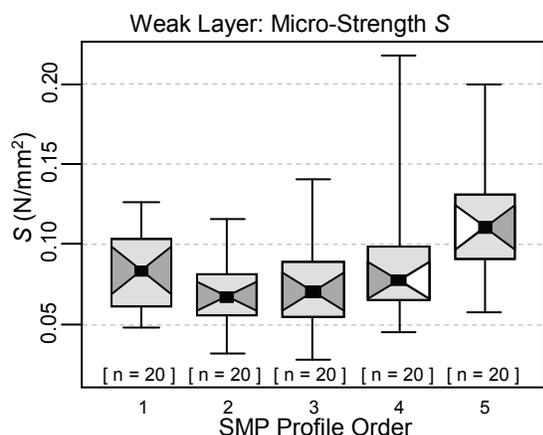
Figure 8. Weak layer micro-strength of Column III, grouped by sample (SMP profile) order (approximately 8 minutes between profiles).

3.7 *Effectiveness of Individual SMP Profiles at Identifying Changes Due to Loading Event*

The profile-based Wilcoxon Tests reveal that each profile from the unstable column (III) produced significantly ($p <= 0.05$) lower S values than each profile in both stable columns (I and II) (Table 3). This means that for this field study only one profile would be necessary per column to identify that a significant decrease in micro-strength occurred in the artificially loaded column. This high degree of representativity would not be expected for thin weak layers, where less microstructural information is recorded, or for smaller loading events. These more subtle conditions are examined by Lutz (in preparation).

Table 3. Count and percentage of profile comparisons yielding results that are representative of the column results.

Expected change due to loading (based on column comparisons):	Was the expected change observed in profile comparisons?	
	Yes Count (%)	No Count (%)
Significant ↓ of f	49 (98%	1 (2%)
Significant ↑ of L	41 (82%)	9 (18%)
Significant ↓ of S	50 (100%)	0 (0%)

4. CONCLUSIONS

4.1 *Observed Phenomena*

Microstructural profiles and boxplot comparisons indicate that distinct differences in *L*, *f*, and *S* existed in the weak layer under different loads. Increasing stress by adding an artificial load caused *f* and *S* to decrease, and resulted in an apparent increase of *L*. Viewed over a short time window, *L* appears to slightly decrease which may be evidence of strengthening.

Decreasing slab stress by removing much of the natural slab coincides with slight increases in *f* and *L*. While the overall micro-strength *S* did not change, these two observed changes may be the result of elastic rebound. Under a reduced load, elastic deformation of microstructures would be reduced, returning the structures to a state of less stress and strain, evident in increased of *f* and L, respectively. On a larger note, elastic deformation persists within the weak layer days after loading events.

Changes in *f* occur at the same force magnitude as the calculated slab force, suggesting that the two phenomena may be related. To our knowledge, this is the first evidence that explicitly shows that changes in weak layer strength occur at the same magnitude as changes in slab stresses related to a loading event. Large significant changes in *S* indicate that this microstructural estimate may be a good indicator for changes in weak layer residual strength, which plays a large role in snowpack stability. For thick weak layers and large loading events, fewer profiles may be necessary to characterize changes in micro-structure than are needed for thin weak layers and small loading events.

4.2 *Field Method*

This field technique is useful for obtaining microstructural estimates of existing stratigraphic features under varying loads. It can be applied over larger time frames as well, to deduce rates of strengthening or weakening. For near-surface instabilities, testing on flat terrain may be easier and allow for properties of the entire slab to be recorded. Most importantly, this field test allows us to record changes in microstructural properties associated with instabilities long before or after any natural instability exists. Researchers can identify changes in microstructure associated with instabilities and, with enough datasets, should be able to calibrate the recorded values to stability indices.

Despite these interesting results, the SMP and other penetrometers will not replace existing testing techniques, but will rather strengthen the diverse tools employed by

researchers and practitioners. Haefeli, who developed the Ramsonde and recognized the potential of improving penetrometer technology (e.g. Bradley, 1966:260), warned of overrating any one observation type: "The factors determining avalanche danger are of such diverse nature, that each method which measures only one characteristic of the snowpack must be considered partial and therefore insufficient" (transl. Bader et al., 1939:150).

4. ACKNOWLEDGEMENTS

5. REFERENCES

Bader, H.P., R. Haefeli, E. Bucher, J. Neher, O. Eckel, C. Thams. 1939. Der Schnee und seine Metamorphose. Beitraege zur Geologie der Schweiz, Geotechnische Serie, Hydrologie Lieferung 3. Kümmerly & Frey, Zürich, 340 pp.

Birkeland, K., K. Kronholm, M. Schneebeli, C. Pielmeier. 2003. Temporal changes in the shear strength and hardness of a buried surface hoar layer. Annals of Glaciology, Vol. 38.

Bradley, C. D. 1966. The Snow Resistograph and Slab Avalanche Investigations. International Symposium on Scientific Aspects of Snow and Ice Avalanches. April 5th – 10th, 1965: Davos, Switzerland. International Union of Geodesy and Geophysics (IUGG) and International Association of Scientific Hydrology (IASH); Commission of Snow and Ice. Pub. No. 69.

Brown, R., K. Birkeland. 1990. A comparison of the digital Resistograph with the ram penetrometer. Proceedings International Snow Science Workshop, Bigfork, MT, USA. 19-30.

Colbeck, S.C., E. Akitaya, R. Armstrong, H. Gubler, J. Lafeuille, K. Lied, D. McClung, and E. Morris. 1990. International Classification for Seasonal Snow on the Ground. International Commission for Snow and Ice (IAHS), World Data Center A for Glaciology, University of Colorado, Boulder, CO, USA.

DeQuervain, M. 1950. Die Festigekeitseigenschaften der Schneedecke und ihre Messung. Geofisica Pura e Applicata, 18: 15.

Dowd, T., R.L. Brown. 1986. A new instrument for determining strength profiles in snow cover. Journal of Glaciology. Vol. 32:111, 299-301.

Greene, E., Birkeland, K.W., Elder, K., Johnson, G., Landry, C., McCammon, I., Moore, M., Sharaf, D., Sterbenz, C., Tremper, B., Williams, K., 2004. Snow, Weather, and Avalanches: Observational Guidelines for Avalanche Programs in the United States. The American Avalanche Association. Pagosa Springs, CO. pp 136. .

Johnson, J., M. Schneebeli. 1999. Characterizing the micro-structural and micromechanical properties of snow, Cold Reg. Sci. Technol., 30: 91–100

Kronholm, K. 2004. Spatial variability of snow mechanical properties with regard to avalanche formation. Doctoral dissertation. Mathematics and Natural Sciences Faculty, University of Zurich, Switzerland. pp. 187.

Lutz, E., Birkeland, K.W., Kronholm, K., Hansen, K., Aspinall, R., 2007. Surface hoar characteristics derived from a snow micropenetrometer using moving window statistical operations. Cold Reg. Sci. Techol., 37 (3): 393-405.

Marshall, H.P. J. Johnson, submitted. Accurate inversion of snow micropenetrometer signals for microstructural and micromechanical properties. Journal of Geophysical Research - Earth Surface.

Paulcke, W., 1938. Praktische Schnee- und Lawinenekunde. Verlag Julius Springer, Berlin, pp. 218.

Pielmeier, C. 2003. Textural and mechanical variability of mountain snowpacks. Doctoral dissertation. Natural Sciences Faculty, University of Bern, Switzerland. pp. 127.

Pielmeier, C., Marshall, H.P, Schweizer, J., 2006. Improvements in the application of the SnowMicroPen to derive stability information for avalanche forecasting. Proceedings International Snow Science Workshop 2006, Telluride CO, USA. 187-192.

Schneebeli, M., J. Johnson. 1998. A constant-speed penetrometer for high-resolution snow stratigraphy. Ann. Glaciol., 26: 107–111.

Schneebeli, M., C. Pielmeier, J. Johnson. 1999. Measuring snow microstructure and hardness using a high resolution penetrometer. Cold Reg. Sci. and Technol., 30 (1-3): 101-114.

Welzenbach, W. 1930. Untersuchungen ueber die Stratigraphie der Schneeablagerungen und die Mechanik der Schneebewegungen nebst Schlussfolgerungen auf die Methoden der Verbauung. Wissenschaftliche Veröffentlichung des Deutschen und Österreichischen Alpenvereins, 9: 114.